

# Unsupervised detection and open-set classification of fast-ramped flexibility activation events

Nils Müller<sup>a,\*</sup>, Carsten Heinrich<sup>a</sup>, Kai Heussen<sup>a</sup> and Henrik W. Bindner<sup>a</sup>

<sup>a</sup>Center for Electric Power and Energy, Technical University of Denmark, Elektrovej, Building 325, 2800 Kgs. Lyngby, Denmark

## ARTICLE INFO

**Keywords:**  
Flexibility  
Event detection  
Open-set classification  
Active distribution grids  
Machine learning  
Electrification

## ABSTRACT

The continuous electrification of the mobility and heating sector will introduce new challenges to distribution grid operation. Uncoordinated activation of flexible units, e.g. simultaneous charging of electric vehicles as a reaction to price signals, could systematically trigger transformer or line protections. Real-time identification of such fast-ramped flexibility activations would allow taking counteractions to avoid potential social and financial cost. In this work, a novel data processing pipeline for identification of fast-ramped flexibility activation events is proposed. The pipeline combines techniques for unsupervised event detection and open-set classification. The systematic evaluation on real load data demonstrates that main building blocks of the proposed pipeline can be realized with methods that fulfill important requirements for an application in a distributed event detection architecture. For the detection of flexibility activation events an upper performance limit is identified. Moreover, it is demonstrated that application of an open-set classifier for classification of flexibility activation events can improve the performance compared to widely-applied closed-set classifiers.

## 1. Introduction

Renewable electricity and electrification are key pillars of global efforts to eliminate carbon in the energy supply. The European goal of carbon neutrality in 2050 is reported to require further increased shares of renewable energy and continued electrification of the mobility and heating sectors [1]. This trend will further increase uncertainty and volatility in distribution grids (DGs). Traditionally designed for the supply of consumers based on centralized generation, DGs turn into carriers of bidirectional power flows [2]. Thus, active management of DGs based on the emerging smart solutions for monitoring, control, and communication is seen as a requirement for distribution system operators (DSOs) [3]. Historically, flexibility for balancing consumption and generation in the power system has been provided on the generation side in a centralized manner. More recently, with the improving capability and affordability of information and communication technology the utilization of local consumption flexibility, commonly referred to as demand response, is becoming more attractive. By reducing equipment loading during peak hours DSOs can use local flexibility to avoid or postpone grid reinforcements [4]. At the same time, DSOs are not aware of all flexibility activations (FAs) affecting their network. Controllable heat pumps and electric vehicles, may systematically react to price signals with a sudden change of power consumption which may result in higher coincidence factors in active DGs [5]. If undetected, such fast-ramped FA events could systematically trigger transformer or line protections. The resulting disconnection of customers could lead to high social and financial cost. The increasing deployment of measurement devices, such as micro phasor measurement units ( $\mu$ PMUs) and smart meters (SMs), in-

crease observability of DGs and thus provide the data basis for identification of FA events. However, real-time identification of FA events is challenged by different practical problems. The infrequent occurrence of FA events limits the available data required for implementation of supervised detection methods. Moreover, the operation of active DGs is influenced by a variety of rare or even unseen event types such as line faults, topology changes or communication failures [6, 7]. Thus, FA event identification also requires differentiation between unknown event classes and FA events. This questions the use of traditional closed-set (CS) classifiers that will falsely classify unknown event classes, due to their inability of rejecting unseen event types. Another challenge for real-time FA event identification is seen in the central data processing, e.g. via cloud computing. Already today the integration of SM data in real-time power system operation is limited by communication instead of meter recording capability [8]. Upgrading communication networks has a high economic burden. Moreover, long communication paths increase the possibilities for false data injection attacks and other fraudulent modification of data [9]. Finally, public clouds are often located abroad, which increases the risk of privacy violations and data leakage of private power readings. One approach to overcome the drawbacks of central data processing is seen in a distributed event identification architecture based on edge or fog computing [10].

The described challenges set specific requirements to the approach and implemented techniques for FA event identification. However, a formulation of these requirements is missing which complicates the development of appropriate strategies and methods for identifying FA events.

In this work, a novel data processing pipeline for the identification of fast-ramped FA events is proposed. A schematic overview of the proposed pipeline is depicted in Fig. 1. The data processing pipeline is based on unsupervised detection and open-set (OS) classification algorithms, suitable

\*Corresponding author

[nilmu@elektro.dtu.dk](mailto:nilmu@elektro.dtu.dk) (N. Müller)

ORCID(s): 0000-0002-3749-5073 (N. Müller)



**Figure 1:** Schematic overview of the proposed event identification pipeline (EIP) for FA events in active DGs.

for application in a distributed event identification architecture. The scheme and algorithm selection is based on a thorough requirements analysis. The core contributions of this work are the systematic selection of processing algorithms and their validation on real load and FA event data.

## 1.1. Related work

The literature on FA event detection and classification is limited. To the best of the authors' knowledge this is the first work on detection and classification of FA events. Thus, in a first step works on thematically related topics are presented, followed by a presentation of methodologically related works. In both cases literature on detection and classification is discussed separately.

### 1.1.1. Thematically related works

A frequently studied topic in power system literature is unsupervised anomaly detection in energy time series data. To detect anomalies most works train models predicting normal behaviour. A data point is declared an anomaly if deviation between the model prediction and the ground truth data exceeds a predefined threshold. Various models such as Variational Autoencoder [11], Hierarchical Temporal Memory (HTM) [12], Autoregressive Integrated Moving Average (ARIMA) or Long Short-Term Memory [13] are applied. None of the works consider FA events as anomaly. Moreover, most works assume anomaly-free training data for learning of the normal behaviour. Some work exists on flexibility detection on building or device level. Authors try to quantify the flexible load potential in load data of individual devices or buildings [14, 15]. Although the name suggest similarity, the problem under investigation is different to the present work.

The topic of event classification in DGs based on  $\mu$ PMU data [16] has been studied intensely. Most works investigate the multi-class CS classification problem. Literature, considering the OS classification problem in a power system context is rare. Mitiche et al. [17] developed a two-stage classifier for fault type identification based on electromagnetic interference diagnostics for high voltage electrical power assets. In the first stage a 1D-Convolutional Neural Network (CNN) filters the relevant in-distribution signals from out-of-distribution signals. The retrieved in-distribution fault signals are then passed to a fault type classifier. To the best of the authors' knowledge, the literature provides no work considering event classification in active DGs as an OS classification problem. With respect to the proposed data processing pipeline, some works on classification in  $\mu$ PMU

data exist that assume an upstream detection step [18, 19]. However, none of these works describe how input samples for the classifier are generated based on the detector results and rather investigate event classification for existing samples.

### 1.1.2. Methodologically related works

Similar to literature on anomaly detection in energy time series data, multiple works propose forecasting-based unsupervised anomaly detection [20, 21, 22]. In most cases, the euclidean distance between point forecast and ground truth is used to flag anomalies based on a defined threshold. In [23] the authors propose the use of a CNN as the time series forecaster. According to the authors, the proposed method can be trained on comparatively small training data and without removing anomalies from the training dataset. A novel approach on anomaly detection in time series data is proposed in [24]. The authors introduce the use of the Spectral Residual (SR) algorithm from saliency detection in computer vision for unsupervised anomaly detection in time series.

In contrast to the traditional CS classification problem, less literature exists on OS classification. Scheirer et al. [25] first formalized the OS classification problem and proposed the 1-vs-Set Machine as a preliminary solution. Since then various methods such as distance-based [26], margin distribution-based [27] or generation-based [28] OS classifiers were proposed. In [29] the authors provide a systematic categorization of OS classification techniques and compare a number OS classifiers on popular benchmark datasets.

## 1.2. Contribution and paper structure

The main contributions of this work are as follows:

- Introduction of a novel EIP based on unsupervised detection and OS classification
- First work on detection and classification of FA events
- First application of OS event classification to events in active DGs
- Introduction of a performance metric for the evaluation of real-time detection of FA events
- Systematic demonstration and validation of unsupervised detection and OS classification of fast-ramped FA events as the main building blocks of the proposed pipeline based on real load data.

The remainder of the paper is structured as follows: In Section 2 requirements for FA event identification in active

DGs are evaluated and strategies are proposed. Section 3 provides a theoretical description of models and methods. In Section 4 the experimental setup is presented, including the dataset under investigation, data preparation for model development and evaluation, and applied performance metrics. In Section 5 results are presented and discussed followed by a conclusion and a view on future work in Section 6.

## 2. Requirements and strategies for FA event identification

Identifying FA events in active DGs comes with specific requirements not only concerning the general approach, but also the implemented algorithms. Additional requirements at algorithm level are introduced by the consideration of event identification based on a distributed architecture. In the following, identified requirements are presented. Based on the requirements analysis the concept of the proposed EIP for FA events (see Fig. 1) as well as the selection of specific models for event detection and classification as the main building blocks are motivated. A detailed explanation of the implemented models and the proposed pipeline follows in Section 3. The problem is limited to fast-ramped load reduction and load increase FA events with a length of up to 3 hours. Moreover, the aggregated active power load profile is assumed to represent averaged active power measurements on secondary substation level or aggregated SM data collected in a data hub on neighborhood level. In both scenarios a large low-voltage feeder is considered. The core of the concept is the separation of the event identification task into an unsupervised event detection and a supervised classification task, resulting in the proposed EIP. Besides the two main building blocks, an event sampler is required to prepare event observations for the classifier based on the results of the event detector.

### 2.1. Real-time identification

A key requirement for identification of FA events is real-time capability. Real-time identification allows DSOs to take immediate counteractions in cases where FAs could result in critical situations, such as congestions and under or over-voltages. Supervised detection or classification of time series events, respectively, usually requires as input the entire time series sample [30]. For real-time event identification this becomes a fundamental problem. Existing early classification techniques come at the cost of decreased accuracy [30] and are not applicable to an OS classification problem. In the proposed pipeline the problem of prediction delay is addressed by separating event identification into two consecutive steps. The use of an unsupervised, point-wise event detector allows for immediate flagging of abnormal data points in real-time. Although this cannot solve the intrinsic problem of supervised classification being dependent on multiple data points of an event, information extraction is improved. Instead of identifying an event at the end of its occurrence, with the presented EIP DSOs will immediately be aware of

the existence of a deviation from normal operation, followed by an ex-post classification of the event.

### 2.2. Model development based on limited and partly-labeled training data

FAs in active DGs constitute rare events. Thus comprehensive datasets of FA events for supervised methods will be difficult to obtain. The heterogeneity of DGs and flexibility portfolios brings additional challenges for acquiring datasets, since characteristics of FAs will differ for different networks. In contrast, unsupervised event detection does not require datasets of FA events. Instead, most works on unsupervised event detection in energy time series data, such as [11], assume event-free training data to learn a representation of the normal behaviour. However, existing training data will most likely contain events, since manual removing is a time consuming and impractical process [31] and DSOs might not be aware of all FAs (see Section 1). In the proposed pipeline a persistence forecast-based detector is considered, which is not dependant on event-free training data. By applying an unsupervised detector with no demand for event-free training data the dependency on labeled training data is reduced to the classification step. Therefore, compared to an one-step event identification approach, the proposed pipeline maintains event detection capability also in scenarios without labeled training data, maximizing information extraction.

### 2.3. Lightweight models for event identification

As described in Section 1, distributed event identification in an edge or fog computing scheme requires models and methods to be lightweight. The vast number and limited processing power of edge devices as well as the continuously growing amount of data sets time and resource constraints to the development, operation and maintenance of models and methods. Therefore, a key requirements for FA event identification is seen in keeping computational and maintenance efforts, such as periodical re-training, at a minimum. This is considered for the proposed concept in several ways. First of all, the proposed pipeline entirely works with delta encoded data. Delta encoding is a technique for data compression based on differencing sequential data, reducing data communication and storage load [32]. By working with differenced data the proposed pipeline can directly be applied in a system which uses delta encoding for data compression. Both the detection and classification model within the pipeline only retrieve features from the univariate load time series. No additional information such as weather or market price data are considered, reducing the requirement for data communication and the dimensionality of the detection and classification problem. The use of a simple persistence forecast keeps size and computational effort of the proposed detector at a minimum and avoids the need for frequent re-training. In the proposed pipeline the classifier only gets activated if the detector has detected a deviation from normal behavior above a predefined threshold. This event-triggered scheme avoids continuous running of the classifier which reduces the required processing power.

For OS classification the Extreme Value Machine (EVM) model is selected as it comes with several features, making it a comparatively lightweight classifier [27]. EVM is capable of incremental learning which allows for efficient model updating without time and computation intensive re-training. Moreover, the model reduction strategy of EVM discards redundant data points within a class of training points, allowing for limitation of model size and classification time as dataset size increases.

#### 2.4. Handling multiple and unknown event classes

In active DGs a large variety of events with various backgrounds such as faults and switching actions can occur. While in this work the detection performance is evaluated on the basis of fast-ramped FA events, in principle an *unsupervised* detector allows for detection of other fast-ramped events as well.

Although traditional CS classifiers can differentiate between multiple known event classes, introducing new unknown classes will lower the classification performance drastically [29]. Observations of unknown classes are wrongly assigned to one of the classes the classifier was trained on, since CS classifiers do not have the capability of rejecting observations of unknown classes. Given that many events only occur rarely and new events might emerge, e.g. due to changes in grid topology, assuming training data to include sufficient observations to describe all existing events is considered an unrealistic assumption. An important requirement for FA event identification is therefore seen in the capability to differentiate between FA events and other event classes by either recognizing known or rejecting unknown event classes. For that purpose, an OS classifier is specifically selected.

#### 2.5. Extension to new event classes

For many other events, such as high-impedance faults or sensor failures, real-time identification would add additional value to DSOs. However, adding additional identification models for every event would again violate the aforementioned time and resource constraints. For this reason, a central requirement is seen in the capability of a model to be extended to identification of additional events while respecting computational and maintenance effort limitations. The use of an unsupervised event detector allows for the detection of other fast-ramped events beyond the considered FA events. To extend the event identification problem to slow-ramped events, the persistence forecast-based detector needs to be replaced or extended. However, due to the modular fashion of the proposed pipeline an extension to slow-ramped events can be achieved without affecting the subsequent classification step. With regard to the classification step, the implementation of an OS classifier with rejection and incremental learning capability facilitates the extension to new event classes: Rejecting observations of unknown classes allows for automated collection, facilitating the manual preparation of new event classes. Once sufficient observations of a new class are collected, the EVM model enables efficient incorporation under an incremental update mechanism. The

model reduction strategy makes EVM a sparse OS classifier which size can be controlled also under extension with new classes.

### 3. Model description

This section formulates the problem of unsupervised event detection and OS classification and describes the implemented models. Thereafter, the concept of the proposed EIP is explained.

#### 3.1. Unsupervised detection of FA events

In this subsection, the unsupervised event detection problem is formulated. Subsequently, the implemented models for unsupervised event detection are described. The implemented models are HTM, ARIMA, CNN, SR and Persistence detector. Focus of the description is on the respective realization of the mapping function given by either (2) or (3).

##### 3.1.1. Problem formulation

In this work, the unsupervised detection of FA events is formulated as a point anomaly detection problem in univariate time series data. A point anomaly is considered a data point that significantly deviates from its expected value. Given an univariate time series  $\mathbf{X} = \{x_1, x_2, \dots, x_N \mid x_i \in \mathbb{R} \forall i\}$ , a data point  $x_t$  at time  $t$  is declared an anomaly if the distance to the expected value  $\hat{x}_t$  exceeds a predefined threshold  $\tau$ :

$$|x_t - \hat{x}_t| > \tau \quad (1)$$

Although all detectors within this work follow different strategies to calculate the expected value  $\hat{x}_t$ , they are all either explicitly or implicitly based on fitting a model to the normal behavior. Given the univariate time series  $\mathbf{X}$ , all detection models either aim at learning a mapping function  $\Phi$  from historical time steps to the next time step

$$\hat{x}_t = \Phi([x_{t-w}, \dots, x_{t-1}]), \quad (2)$$

or a direct mapping function  $\Theta$  from historical time steps to the anomaly score of the next time step

$$s_t = \Theta([x_{t-w}, \dots, x_{t-1}]), \quad (3)$$

where  $w$  is the size of the history window, which can vary for the different detectors, and  $s_t$  is the predicted anomaly score at time  $t$ . In case of a mapping according to (2) an additional step is required to map  $\hat{x}_t$  to the anomaly score  $s_t$ , while (3) calculates the anomaly score directly.

##### 3.1.2. HTM detector

HTM [33] is a machine learning technique that is based on the structural and algorithmic properties of the neocortex. At its core HTM consists of time-based learning algorithms that learn, store and recall spatial and temporal sequences. HTM uses stored data sequences to predict the next time step according to (2). A key difference of HTM to most other machine learning techniques is the continuous learning capability. HTM adapts to changing statistics of the input data



on the fly in an unsupervised manner and does not require frequent re-training. The implementation of HTM includes an internal calculation of anomaly scores such that the HTM detector overall follows (3). For  $x_t$ , let  $\mathbf{a}(x_t)$  be the sparse encoding of  $x_t$  and  $\pi(x_{t-1})$  be a sparse vector representing the internal prediction of the HTM model of  $\mathbf{a}(x_t)$  [20]. The anomaly score is calculated as

$$s_t = 1 - \frac{\pi(x_{t-1}) \cdot \mathbf{a}(x_t)}{|\mathbf{a}(x_t)|}, \quad (4)$$

where  $|\mathbf{a}(x_t)|$  is the scalar norm of  $\mathbf{a}(x_t)$ . In case of a perfect match, the anomaly score is 0. If the two vectors are orthogonal,  $s_t = 1$ . HTM also calculates the anomaly likelihood  $L_t$  which aims at taking the current prediction error distribution into account to define how anomalous the current state is based on the prediction error history. The anomaly likelihood is defined as the complement of the tail probability according to

$$L_t = 1 - Q\left(\frac{\tilde{\mu}_t - \mu_t}{\sigma_t}\right), \quad (5)$$

with the rolling normal error distribution defined by the mean  $\mu_t$  and variance  $\sigma_t^2$ , that are continuously updated with

$$\mu_t = \frac{\sum_{i=0}^{w-1} s_{t-i}}{w} \quad (6)$$

and

$$\sigma_t^2 = \frac{\sum_{i=0}^{w-1} (s_{t-i} - \mu_t)^2}{w - 1}. \quad (7)$$

$\tilde{\mu}_t$  is a recent short term average of prediction errors defined as

$$\tilde{\mu}_t = \frac{\sum_{i=0}^{w'-1} s_{t-i}}{w'}, \quad (8)$$

with  $w'$  being the size of the history window for short term moving average given  $w' \ll w$ . A threshold  $\tau$  for declaring anomalies can either be applied on the anomaly score  $s_t$  or the anomaly likelihood  $L_t$ . According to [20] using  $L_t$  has advantages in scenarios with inherent randomness or noise, as  $L_t$  takes into account how well the model currently predicts compared to the recent history. In this work, thresholding is applied to  $L_t$ . HTM comes with approximately 30 model configuration parameters. In the supplementary of [20] the authors provide a set of optimal model parameters for anomaly detection which is applied in this work.

### 3.1.3. ARIMA detector

ARIMA models are widely applied for time series forecasting [34]. ARIMA models use previous time steps to forecast future behavior and can be applied to learn a mapping function according to (2). In a subsequent step the difference

between the predicted value  $\hat{x}_t$  and the true value  $x_t$  can be compared to a pre-defined threshold  $\tau$  as given in (1). An ARIMA model consists of an autoregressive (AR), an integrated (I) and moving average (MA) part and is classified as an ARIMA  $(p, d, q)$  model, where  $p$ ,  $d$  and  $q$  define the order of the respective terms. Let  $x_{\Delta,t}^{(d)}$  be the  $d^{\text{th}}$  difference of  $x_t$ , then the forecasting equation is given by

$$\hat{x}_{\Delta,t}^{(d)} = \mu + \sum_{j=1}^p \varphi_j x_{\Delta,t-j}^{(d)} + \epsilon_t + \sum_{j=1}^q \theta_j \epsilon_{t-j}, \quad (9)$$

where  $\varphi_j$  is the  $j^{\text{th}}$  autoregressive parameter and  $\theta_j$  the  $j^{\text{th}}$  moving average parameter. The reconversion from differenced data can be achieved by

$$\hat{x}_t = \hat{x}_{\Delta,t}^{(1)} + x_{t-1} \quad (10)$$

in case of  $d = 1$ . Time series data with a seasonal component is not directly supported by ARIMA models. To overcome this limitation in this work the seasonal pattern is modeled using Fourier terms [35]. Based on (9) and (10) the forecasting equation for seasonal time series with long seasonal periods can be expressed as

$$\hat{x}_{S,t} = a + \sum_{k=1}^F [\alpha \sin(2\pi kt/m) + \beta \cos(2\pi kt/m)] + \hat{x}_t, \quad (11)$$

where  $F$  is the number of Fourier terms and  $m$  the seasonal period of the aggregated load time series with  $m = 288$ .

In this work, auto-ARIMA [36] is used for model selection based on the lowest Akaike information criterion on the first 10 days of the dataset. In a pre-processing step the distribution of the training data is centered on a mean of  $\mu = 0$  and a standard deviation of  $\sigma = 1$ , resulting in a standardization of the data according to

$$z_t = \frac{x_t - \mu_{\text{train}}}{\sigma_{\text{train}}}. \quad (12)$$

After initial training, the autoregressive and moving average parameters  $\varphi$  and  $\theta$  are updated with every new incoming observation. Every 14 days an entirely new ARIMA model is selected based on the Akaike information criterion, resulting in a new selection of  $p$ ,  $d$ ,  $q$  and  $F$ .

### 3.1.4. CNN detector

CNNs [37] are a specialized class of Artificial Neural Networks. The use of CNNs for unsupervised anomaly detection in time series has lately been proposed by Munir et al. [23]. For that purpose, a CNN is applied to forecast the next time step  $x_t$  based on the mapping of previous data points according to (2). By thresholding the difference between the expected value  $\hat{x}_t$  and the true value  $x_t$  as given in (1), data points can be declared as either anomalous or non-anomalous. In Artificial Neural Networks the mapping function in (2) is realized by stacked layers consisting of linear maps and subsequent non-linear transformations. The  $j$ th layer maps its input  $\mathbf{x}_{j-1}$  to the output  $x_j$  according to

$$\mathbf{x}_j = \psi(\mathbf{W}_j \mathbf{x}_{j-1} + \mathbf{b}_j), \quad (13)$$

where  $\mathbf{W}$  represents the weights and  $\mathbf{b}$  biases of the  $j$ th layer, respectively, and  $\psi$  is a non-linear activation function. In case the layer is not the first layer of the network, the input  $\mathbf{x}_{j-1}$  is given by the output of the previous layer. In the convolutional layers of CNNs the linear maps are replaced by convolutional operations. In case of univariate time series forecasting, convolution is applied on an one-dimensional input vector  $\mathbf{x}_{j-1}$  through sliding-window filters. Let  $\omega = (\omega_1, \dots, \omega_w)$  be a set of convolutional filters, then the  $i$ th entry of the output of the  $j$ th layer is

$$\mathbf{x}_j^{(i)} = f\left(\sum_{k=1}^w \omega_k \mathbf{x}_{j-1}^{(i+k)}\right), \quad (14)$$

where  $f$  is a non-linear activation function. A convolutional layer is typically followed by a max-pooling layer that computes the maximum activation of a selected pool of adjacent neurons from the convolutional layer [38, 39]. After sequence of pairs of convolutional and max-pooling layers, a final fully connected layer follows. In the fully connected layer all neurons are connected to each activation of the previous layer as described by (13).

To avoid a local minimum given by the persistence forecast  $\hat{x}_t = x_{t-1}$  and to allow for better investigation of the predictability, the difference  $x_{\Delta,t} = x_t - x_{t-1}$  instead of  $x_t$  is forecasted. In addition, the data is standardized according to (12).

To define the architecture and hyperparameters of the CNN, extensive empirical experiments are conducted based on the first 10 days of the dataset. While the first 7 days are used as an initial training dataset set, the remaining 3 days are used for validation. The resulting CNN architecture consists of three convolutional/max-pooling pairs followed by a fully connected layer. An overview of the main hyperparameters is given in Table 1. After the initial training and model selection phase the CNN is re-trained every 14 days based on the previous data. To avoid overfitting a combination of early stopping, L2 regularization and dropout is applied. The corresponding hyperparameters of the regularization techniques are listed in Table 1.

### 3.1.5. SR detector

SR [40] is an unsupervised algorithm for visual saliency detection in computer vision. Saliency is defined as contrast of features such as color or intensity, and can be thought of what "stands out" in a picture [41, 42]. Recently, Ren et al. [24] proposed the use of SR for unsupervised anomaly detection in time series data, motivated by the similarity of time series anomaly detection and visual saliency detection. The SR algorithm calculates a so-called saliency map  $\mathcal{S}(\mathbf{x})$  of a sequence  $\mathbf{x} = \{x_1, x_2, \dots, x_N\}$  in three main steps. First the log amplitude spectrum of  $\mathbf{x}$  is calculated based on Fourier transform. In a second step, the spectral residual of the log amplitude spectrum is determined followed by an inverse Fourier transform to reconvert the spectral residual of  $\mathbf{x}$  to the spatial domain, resulting in the saliency map  $\mathcal{S}(\mathbf{x})$ . Similar to the previously described detectors the SR algorithm performs a mapping of previous data points to the next time

**Table 1**

Summary of hyperparameters of the CNN model.

| Hyperparameter                       | Search space        | Selected value |
|--------------------------------------|---------------------|----------------|
| History window size                  | 144, 288, 576, 1152 | 288            |
| Forecasting horizon                  | 1                   | 1              |
| Learning rate                        | [0.00001, 0.1]      | 1e-5           |
| L2 weight regularization             | [0.0001, 0.1]       | 0.01           |
| Dropout rate                         | [0, 0.2]            | 0.2            |
| Batch size                           | 10, 50, 100, 500    | 50             |
| Maximum number of epochs             | 2000                | 2000           |
| Number of filters                    | 10, 30, 50, 70      | 50             |
| Kernel size                          | 2, 3, 4             | 3              |
| Neurons in the fully connected layer | 10, 50, 100, 150    | 100            |
| Early stopping patience              | 10, 50, 100         | 50             |
| Activation function                  | ReLU, Sigmoid       | ReLU           |

step according according to (2). However, the mapping is conducted within the saliency map representation of  $\mathbf{x}$  and based on a local average of the saliency map representations of the previous data points within the history window size  $w$ :

$$\begin{aligned} \hat{S}_t &= \phi(\{S_{t-w}, \dots, S_{t-1}\}) \\ &= \frac{S_{t-1} + S_{t-2} + \dots + S_{t-w}}{w} \end{aligned} \quad (15)$$

Similar to (1) the declaration of anomalous data points can now be conducted based on thresholding the difference between the predicted and actual value of the saliency map representation of  $x_t$ :

$$|S_t - \hat{S}_t| > \tau \quad (16)$$

The capability of the SR algorithm to detect anomalous data points is improved when the data point under investigation is located in the center of the sequence  $\mathbf{x}$ . However, as this work is concerned with real-time detection of FA events, the SR algorithm is used to declare only the most recent data point  $x_N$  of sequence  $\mathbf{x}$  either as anomalous or non-anomalous. Ren et al. [24] propose to add estimated data points following  $x_N$  by

$$\bar{g} = \frac{1}{w'} \sum_{i=1}^{w'} g(x_N, x_{N-i}) \quad (17)$$

$$\hat{x}_{N+1} = x_{N-w'+1} + \bar{g} \cdot w', \quad (18)$$

with  $g(x_N, x_{N-i})$  being the gradient of the linear connection between  $x_N$  and  $x_{N-i}$  and  $\bar{g}$  representing the average gradient of the  $w'$  preceding points with  $w' \ll w$ . Ren et al. further propose to fill all following values  $\hat{x}_{N+1}, \dots, \hat{x}_{N+r}$  with the estimated value  $\hat{x}_{N+1}$  according to (18).

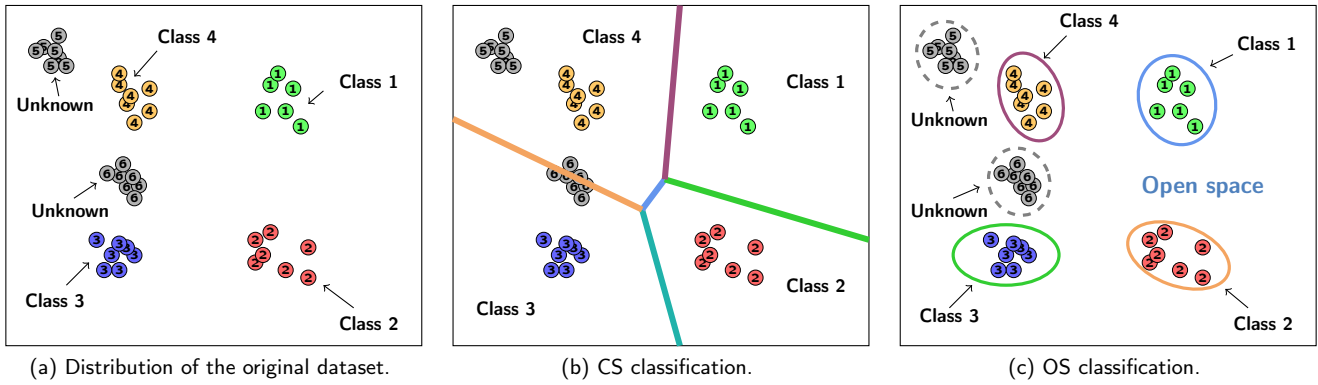


Figure 2: Comparison of CS and OS classification according to [29].

### 3.1.6. Persistence detector

Within this work, the use of a persistence forecast for modeling the expected value  $\hat{x}_t$  is proposed and compared to more sophisticated forecasting methods. The proposed Persistence detector considers a history window  $w = 1$  and determines  $\hat{x}_t$  according to

$$\hat{x}_t = x_{t-1}. \quad (19)$$

The triviality of the Persistence detector reduces hyperparameter tuning to the selection of the threshold  $\tau$ .

## 3.2. OS classification of FA events

This subsection first formulates the OS classification problem. Subsequently, theory and implementation of the selected OS classifier are described.

### 3.2.1. Problem formulation

OS classification is contrasted with CS methods typically applied in the literature. CS classification considers the same types and number of event classes in training and test data and thus assumes full awareness of all existing event classes. For DSOs it might be difficult or even impossible to obtain data comprising observations off all existing event classes, since events such as failures of transmission elements, large DERs or sensors might occur for the first time. For example, a CS classifier trained on observations of line failures and capacitor bank switching actions declares every observation of an unknown event class as either a line failure or a capacitor bank switching action. An OS classifier rejects observations of event classes not previously seen and declares them as "unknown". In Fig. 2 CS classification is compared to OS classification. Making CS assumptions leads to regions of unbounded support, as can be seen from Fig. 2 (b). Under existence of unknown classes, this results in missclassification of observations from unknown classes which can drastically weaken the robustness and performance of the classification.

According to Yu et al. [43], the problem of OS classification can be formulated as follows. Let  $\mathbf{D}_{\text{train}} = \{(\mathbf{v}_i, y_i)\}_{i=1}^{N_{\text{train}}}$  be a training dataset, with  $\mathbf{v}_i \in \mathbb{R}^d$  being a feature vector

instance and  $y_i \in \mathbf{Y}_{\text{train}} = \{1, 2, \dots, K\}$  the corresponding event class label. During the test or application phase a classifier needs to predict event classes of the open dataset  $\mathbf{D}_o = \{(\mathbf{v}_i, y_i)\}_{i=1}^{\infty}$ , where  $y_i \in \mathbf{Y}_o = \{1, 2, \dots, K, K+1, \dots, M\}$  with  $M > K$ . The occurrence of unknown classes requires the classifier to learn a mapping function  $f(\mathbf{v}) : \mathbf{V} \rightarrow \mathbf{Y}' = \{1, 2, \dots, K, \text{unknown}\}$ , with the option *unknown* representing the rejection of classes not seen during training, by minimizing the expected risk according to

$$f^* = \arg \min_{f \in \mathcal{H}} \mathbb{E}_{(\mathbf{v}, y) \sim \mathbf{D}_o} [\text{err}(y, f(\mathbf{v}))], \quad (20)$$

where  $\mathcal{H}$  is the hypothesis space of a fixed class of functions and *err* is given by

$$\text{err}(y, f(\mathbf{v})) = \begin{cases} 1 & \text{if } f(\mathbf{v}) \neq y, & \text{for } y \in \mathbf{Y} \\ 0 & \text{if } f(\mathbf{v}) \neq \text{unknown}, & \text{for } y \notin \mathbf{Y} \end{cases}. \quad (21)$$

### 3.2.2. EVM classifier

The EVM is an OS classifier proposed by Rudd et al. [27]. EVM can perform nonlinear, kernel-free classification, supporting variable bandwidth incremental learning in a multi-class OS scenario. The EVM models known classes within the training dataset by a set of extreme vectors. Each extreme vector is affiliated with a radial inclusion function  $\Psi$  modeling the probability of sample inclusion. The functional form for  $\Psi$  is derived from the concept of margin distributions and its extension from a per-class to a sample-wise formulation.  $\Psi$  is modeled in terms of the distribution of sample half-distances relative to a reference point. Specifically, the EVM applies the following marginal distribution theorem:

**Theorem 1.** *Assume we are given a positive sample  $v_i$  and sufficiently many negative samples  $v_j$  drawn from well-defined class distributions, yielding pairwise margin estimates  $\tilde{m}_{ij}$ . Assume a continuous non-degenerate margin distribution exists. Then the distribution for the minimal values of the margin distance for  $v_i$  is given by a Weibull distribution.*

Given that the marginal distribution theorem holds for any point  $v_i$ , each point can estimate its respective distribution of distance to the margin, resulting in:

**Corollary 1.1. ( $\Psi$  Density Function)** Given the conditions for the Theorem 1, the probability that  $v'$  is included in the boundary estimated by  $v_i$  is given by

$$\Psi(v_i, v', \kappa_i, \lambda_i) = \exp\left(-\left(\frac{\|v_i - v'\|}{\lambda_i}\right)^{\kappa_i}\right), \quad (22)$$

where  $\|v_i - v'\|$  is the distance of  $v'$  from sample  $v_i$ , and  $\kappa_i$  and  $\lambda_i$  are Weibull shape and scale parameters respectively obtained from fitting to the smallest  $\tilde{m}_{ij}$ .

The radial inclusion function  $\Psi$  provides a rejection model where the probability of inclusion is given by the probability of the sample not laying well into or beyond the negative margin.

After training the EVM, the probability of a new observation  $v'$  belonging to class  $C_l$  can be determined by

$$\hat{P}(C_l|v') = \max_{\{i: y_i=C_l\}} \Psi(v_i, v', \kappa_i, \lambda_i). \quad (23)$$

Based on the threshold  $\rho$  defining the boundary between the set of known classes  $\mathcal{C}$  and the unknown open space the classification decision function is

$$y^* = \begin{cases} \arg \max_{l \in \{1, \dots, M\}} \hat{P}(C_l|v') & \text{if } \hat{P}(C_l|v') \geq \rho \\ \text{"unknown"} & \text{Otherwise} \end{cases}. \quad (24)$$

The number of input features of the classifier is limited to 6. As described before it is unlikely that DSOs will have comprehensive labeled datasets of most event classes due to their rare occurrence. Also in the present dataset the number of FA events is comparatively small. Reducing the dimension of the feature space that needs to be described by the limited number of training observations allows for better determination of the radial inclusion functions  $\Psi$ . All features are derived from the delta encoded time series and are listed in Table 2. The definition of the input features is given based on a sequence observation  $\mathbf{x} = \{x_1, \dots, x_{N_x}\}$ .

**Table 2**  
Overview of features used for OS classification of FA events.

| Feature   | Definition  |
|---|---|
| Mean $\mu_x$  | $\frac{1}{N_x} \left( \sum_{i=1}^{N_x} x_i \right)$       |
| Standard deviation $\sigma_x$                           | $\sqrt{\frac{1}{N_x-1} \sum_{i=1}^{N_x} (x_i - \mu_x)^2}$ |
| Minimum value $x_{\min}$                                | $\min(\mathbf{x})$  |
| Maximum value $x_{\max}$                                | $\max(\mathbf{x})$  |
| Number of zeros $n_0$                                   | $\text{count}(\mathbf{x} \stackrel{!}{=} 0)$              |
| Points between minimum and maximum value $n_{\min\max}$ | $ \text{index}(x_{\min}) - \text{index}(x_{\max}) $       |

The EVM model training and selection is based on 90 % of the available event observations applying 5-fold time series cross-validation. The features are standardized based on training data for every individual split according to (12). In order to selected an appropriate threshold  $\rho$  a minimum performance requirement on the training dataset is defined based on the  $F_1$  score performance metric (Subsection 4.2).

**Table 3**  
Summary of hyperparameters of the EVM model.

| Hyperparameter      | Search space   | Selected value    |
|---------------------|--|-------------------|
| Tailszie            | [1,100]  | 7                 |
| Distance multiplier | [0.1,1.1]  | 0.9               |
| Distance metric     | Canberra distance,<br>Cosine distance,<br>Euclidean distance | Canberra distance |
| Threshold           | [0.1, 0.99999]   | 0.9               |

The model with the smallest threshold  $\rho$  which still fulfills the performance requirement  $F_1 \geq 0.8$  in the time series cross-validation is selected. An overview of the selected hyperparameters is given in Table 3.

### 3.3. EIP

To connect the presented models for unsupervised event detection and OS classification, a data processing pipeline is proposed. In Fig. 1 a schematic overview of the EIP is depicted. The functionality of the main building blocks of the pipeline was described in Subsection 3.1 and 3.2. In Subsection 2.3 the use of delta encoded data for the EIP was motivated. Delta encoding exploits the autocorrelation of time series data. In the simplest version of delta encoding a time series  $\mathbf{X} = \{x_1, x_2, \dots, x_{N_x}\}$  is encoded as difference between successive samples, resulting in the delta encoded time series  $\mathbf{X}_\Delta = \{x_1, x_2 - x_1, \dots, x_{N_x} - x_{N_x-1}\} = \{x_1, x_{\Delta,2}, \dots, x_{\Delta,N_x}\}$ . Delta encoding performs best when the values in the original data contain only small changes between adjacent values [44]. By applying the Persistence detector on the delta encoded time series  $\mathbf{X}_\Delta$  the anomaly detection problem reduces to comparison of the amplitudes of  $x_{\Delta,i}$  to the predefined threshold  $\tau$ . To connect point-wise unsupervised event detection with OS classification, an event sampler is interposed, exploiting the characteristics of fast-ramped events. As can be seen in Fig. 4 fast-ramped FA events show peaks in the delta encoded data at the beginning and/or end of an event. Based on this property, the detection of an event at data point  $x_{\Delta,t}$  can be used to extract a backward sequence sample  $\mathbf{x}_{\Delta,bw} = \{x_{\Delta,t-w_x}, \dots, x_{\Delta,t+e}\}$  and forward sequence sample  $\mathbf{x}_{\Delta,fw} = \{x_{\Delta,t-e}, \dots, x_{\Delta,t+w_x}\}$  where  $w_x$  is the sample window size and  $e$  a window extension, ensuring sampling of the entire event. In case of forward sampling, an early stopping criterion can be introduced which breaks the sampling process in case another event is detected at a data point  $x_{\Delta,t+a} \in \{x_{\Delta,t+1}, \dots, x_{\Delta,t+w_x}\}$ , resulting in a forward sample  $\mathbf{x}_{\Delta,fw} = \{x_{\Delta,t-e}, \dots, x_{\Delta,t+a+e}\}$ . Such event-triggered early stopping of the forward sampling process reduces the sampling time and thus the time until a sample can be classified. In the Appendix in Algorithm 1 the general procedure of the proposed EIP is described.



## 4. Experimental setup

This section presents the experimental setup of this study. The considered dataset as well as the preparation of the dataset for investigation of unsupervised event detection and OS classification of FA events are presented in Subsection 4.1. Subsection 4.2 introduces metrics for the evaluation of the detection and classification performance.

### 4.1. Dataset and data preparation

The first part of this subsection is concerned with presenting key information of the dataset under investigation as well as describing the process of FA. In the second part the preparation of the dataset is explained, which includes data cleaning and in case of preparation for the investigation of the OS classification the extension of the dataset with two artificial event classes.

#### 4.1.1. Dataset

Within this work, a dataset from EcoGrid 2.0 is used. EcoGrid 2.0 was a demonstration project which examined the use of flexible consumption of residential customers for power system services at transmission system operator and DSO level [45]. The experiments were conducted on the Danish island of Bornholm. The residential costumers were equipped with SMs and information and communication technology infrastructure for participating in the demand response experiments. The flexible load is given by electric heaters and heat pumps that have been controlled by adjusting room temperature setpoints or a throttle signal, respectively. An increase in the setpoints results in a higher consumption, while lowering the setpoints leads to a reduction of consumption. Besides the flexible load, the installed SMs also capture household consumption and potentially photovoltaic production. As can be seen in Fig. 3 (a), the dataset used in this work consists of six and a half months of aggregated load data, beginning from 15<sup>th</sup> of September 2017. The aggregated active power profile consists of 450 household loads and is represented in 5 minutes intervals. The FA events consist of load reduction and load increase experiments (see Fig. 3 (b)) realized by two different aggregators and customer portfolios. Activation periods are in the range of 30-120 minutes. The FAs are based on different numbers of customer loads and were conducted under varying conditions of temperature, time of the day and photovoltaic production. Fig. 3 shows the trend and seasonal component of the non-stationarity load time series.

#### 4.1.2. Dataset preparation for investigation of unsupervised event detection

The dataset contains 325 FA events. Start and end time as well as type of FA event is known for every experiment. In 75 cases two flexibility portfolios were activated simultaneously. To avoid double counting of either true positives (TPs) or false negatives (FNs) parallel experiments are considered as one FA event, reducing the number of FA events to 250. In most cases the experiments go along with either

load reduction or load increase of a subset of the customer loads. However, in some cases no or almost no flexibility was activated. This can be due to exclusive testing of connectivity, failed activation of flexibility assets or low flexibility potential due high temperatures and thus low heating demand. Such false or minor activations complicate the evaluation of the detection performance. Considering undetected false activations as FNs wrongly results in a poorer detection performance. However, removing false or minor activations may wrongly increase the detection performance as some FAs are removed that potentially could be detected, albeit difficult. Both approaches will bias the detection performance in one or the other way. For this work, only FA events that the authors could manually detect without knowledge of the event labels are considered, reducing the number of FA event samples to 205. This approach limits the investigation of FA events to the detection of events that could be manually detected by operators with high knowledge of the system in an extensive ex-post evaluation of historical load data. However, as the motivation of the proposed concept for FA event detection and classification is the early detection of potentially critical FAs, neglecting unnoticeable activations is seen as the less distorting intervention.

#### 4.1.3. Dataset preparation for investigation of OS event classification

In Fig. 4 examples of all event classes are depicted in absolute and delta encoded values. Note that only for the OS classification problem all introduced event classes are considered. For the FA event detection problem only FA events are taken into account. The classifier is trained on two known event classes, namely FA and normal operation (NO) events. All 205 FA events are sampled, including 3 timestamps (15 minutes) before the start and after the end of an event, respectively. As the duration of FA events varies, the length of FA event samples varies as well. An equal amount of NO events are randomly sampled from the remaining dataset. The length of a NO event is randomly selected from the distribution of FA event lengths. With this approach, the classifier is prevented from differentiating between FA and NO events based on the sample length. As the sample length of both FA and NO events can vary in the proposed EIP (see Subsection 3.3) learning a constant sample length is not considered a valid approach.

The problem of OS classification, as formulated in Subsection 3.2.1, requires additional event classes within the test dataset, to investigate the capability of rejecting unknown classes. In this work, 3 unknown event classes are considered. Besides the FA and NO event classes, the EcoGrid 2.0 dataset includes another event class, which in the course of this work will be called Monday peak (MP). On every Monday within the dataset, a load peak occurs at around 8 am. The load peak results from short, collective heating of electric heaters to 80 °C in order to inhibit the growth of bacteria. According to the FA events, only MP events that could be manually detected in an extensive ex-post evaluation of the dataset are considered. MP events are not considered a nor-

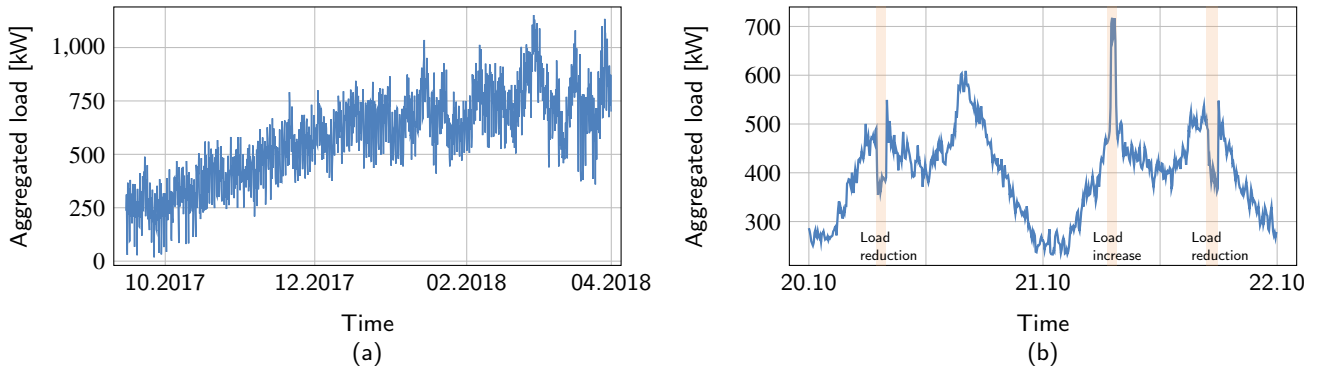


**Figure 3:** Aggregated load dataset (a) and aggregated load of two representative days with frequent FAs (b). Periods of FAs are marked with an orange background.

mal operation and thus no overlapping of NO and MP events exists. In total the dataset includes 15 MP events. In order to extend the OS classification problem, two additional artificial event classes are introduced, namely the frozen value (FV) and data unavailability (DU) event class. The FV event class models a data transmission or processing failure in which a measurement at time  $t_0$  remains constant for  $N_{\text{cons}}$  consecutive steps. At  $t_{N_{\text{cons}}+1}$  recording of the true measurement is reestablished. The length of FV events is randomly selected from the same distribution as the length of FA events. 205 FV events are randomly introduced into the subset of the dataset which is not influenced by FA, NO and MP events. In a DU event a subset of individual measurements, e.g. SM readings, is considered to be unavailable due to device or data transmission failure. The fraction of available measurements is randomly selected from the uniform distribution  $\mathcal{U}(0.4, 0.8)$ . Equivalent to NO and FV events the length of DU events is randomly drawn from the distribution of FA event lengths. 205 DU events are introduced into the subset of the dataset not affected by any of the previously described events.

## 4.2. Performance metrics

The performance evaluation of both the unsupervised detection and OS classification of FA events is based on a labeling of each instance of the respective dataset. The definition of an instance for the detection and classification task, respectively, follows in Subsection 4.2.1 and 4.2.2. One performance metric used for evaluation of both the detection and classification part is the so-called  $F_1$  score. The  $F_1$  score represents the harmonic mean between precision and recall and is a widely applied performance metric for detection and classification problems with imbalanced classes. Let  $TP_l$ ,  $FP_l$ ,  $TN_l$ , and  $FN_l$ , respectively, be the number of TPs, false positives (FPs), true negatives (TNs), and FNs for the  $l$ -th event class, where  $l \in \{1, 2, \dots, M\}$ . For a multi-class problem, the  $F_1$  score is calculated by

$$F_1 = 2 \times \frac{Pr \times Re}{Pr + Re}, \quad (25)$$

where the precision  $Pr$  and the recall  $Re$  are defined as

$$Pr = \frac{\sum_{l=1}^M TP_l}{\sum_{l=1}^M (TP_l + FP_l)}, \quad Re = \frac{\sum_{l=1}^M TP_l}{\sum_{l=1}^M (TP_l + FN_l)}. \quad (26)$$

### 4.2.1. Unsupervised event detection metrics

In this work, the problem of unsupervised event detection is considered an anomaly detection problem, reducing the number of classes to  $M = 2$ . Since anomalies constitute the primary class of interest, the multi-class formulation for precision and recall in (26) reduces to

$$Pr = \frac{TP_1}{TP_1 + FP_1}, \quad \text{and} \quad Re = \frac{TP_1}{TP_1 + FN_1} \quad (27)$$

for calculation of the  $F_1$  score in (25).

Besides the  $F_1$  score, another widely applied performance metric for anomaly detection is the area under the precision-recall curve ( $AUCPR$ ). Precision-recall curves summarize the trade-off between precision and recall for different thresholds  $\tau$ . While the consideration of TNs in traditional receiver-operating-characteristic curves may lead to an overly optimistic view on the performance in case of highly imbalanced classes,  $AUCPR$  is specifically tailored to problems with imbalanced classes or rare events.

In this work, the entire sequence of an FA event, referred to as event window  $\omega_{\text{FA}}$ , is considered for labeling as TP or FN. The event window of a FA event is defined by the FA start time  $t_{\text{FA,start}}$  and end time  $t_{\text{FA,end}}$ . Since the dataset under investigation is a real-world dataset it contains some inaccuracies in the event labeling. In some cases flexibility was activated before the official start time  $t_{\text{FA,start}}$ . Since in these cases an early detection would result in falsely FNs the event window  $\omega_{\text{FA}}$  is extended by 10 minutes, such that  $\omega_{\text{FA}} = \{x_{t_{\text{FA,start}}-2}, \dots, x_{t_{\text{FA,end}}}\}$ . The first detection that falls into  $\omega_{\text{FA}}$  is considered as TP, while further detections within the same event window are ignored. If no point of  $\omega_{\text{FA}}$  is detected the event label will be considered a FN. In most cases, FAs result in a subsequent load rebound, which can be considered a deviation from the normal load behavior outside of the activation period. While regarding a detection within

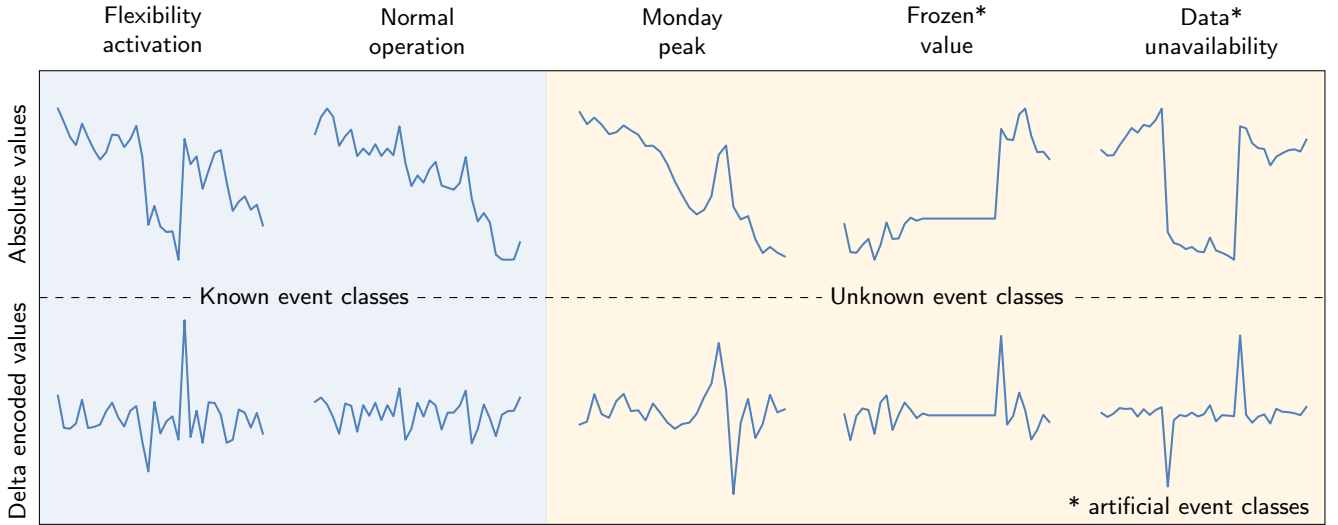


**Figure 4:** Exemplary representation of event classes considered in this work.

the rebound area as TP would introduce a positive bias to the detection performance, considering them as FP would result in overly pessimistic performance results, as the detector indeed has detected an anomaly. For this reason, a rebound window  $\omega_R$  is introduced in which detections are ignored and are thus neither considered a TP nor FP. The length of a rebound window is defined as three times the FA event length, resulting in  $\omega_R = \{x_{t_{FA,end}+1}, \dots, x_{t_{FA,end}+3 \times N_{FA}}\}$ . In contrast to the calculation of TPs and FNs, the calculation of FPs and TNs is conducted point-wise, thus, all detections outside the event and rebound windows are considered FP.

To evaluate the early detection capability, the average detection delay  $\bar{\delta}_{det}$  is introduced as the average time between FA start time  $t_{FA,start}$  and the first detection time  $t_{det}$  in minutes according to

$$\bar{\delta}_{det} = \frac{1}{N_{det}} \sum_{i=1}^{N_{det}} \delta_{det,i} = \frac{1}{N_{det}} \sum_{i=1}^{N_{det}} (t_{det,i} - t_{FA,start,i}), \quad (28)$$

where  $N_{det}$  is the number of detected FA events and  $\delta_{det,i}$  the detection delay of a detected FA event. Note that the detection delay of detections are assumed to be zero within the subset  $\{x_{t_{FA,start}-2}, x_{t_{FA,start}-1}, x_{t_{FA,start}}\}$ .

The use of widely applied performance metrics allows for an easy understanding and comparison of the results to other studies. However, in order to take performance requirements of a specific scenario into account an individual performance metric is required. For this purpose, the flexibility activation detection score (*FAD score*) is proposed. In the scenario of real-time detection of FAs in active DGs, the cost of FN is considered to be higher compared to the cost of FP. While a missed critical FA could lead to violation of power or voltage boundaries, a false alarm would result in a moderate additional manual inspection effort. Moreover, in the proposed pipeline, a FP will lead to a sample of normal behavior (NO event class) which can be classified as such

by the OS classifier. In this way the classifier relativizes the FP of the unsupervised event detector. For these reasons, the *FAD score* puts more weight on FNs than on FPs. Further, early detection capability is an important requirement in the considered scenario. The earlier a potentially critical FA event is detected, the greater the scope for countermeasures. On the contrary, the detection near the end of a critical FA results in almost no benefit. The *FAD score* takes these considerations into account and expresses the performance for the specific scenario of real-time FA event detection in one score. Besides an easier evaluation and comparison of detection models, the *FAD score* also allows for easy selection of an optimal threshold  $\tau$  for unsupervised detection of FA events. The proposed *FAD score* constitutes of 3 scoring functions  $\zeta_{TP}$ ,  $\zeta_{FN}$  and  $\zeta_{FP}$ , representing the contribution of TPs, FNs and FPs, respectively:

$$FAD = \zeta_{TP} - \zeta_{FN} - \zeta_{FP} \quad (29)$$

Let  $x_{t_{FA,start},i}$ ,  $x_{t_{FA,end},i}$  and  $x_{t_{det},i}$  be the start point, end point and first detection within the event window  $\omega_{FA,i}$  of the  $i$ -th FA event, respectively. Then  $\zeta_{TP}$  is given by

$$\zeta_{TP} = \sum_{i=1}^{N_{det}} \sigma_i(x_{t_{det},i}), \quad (30)$$

where  $\sigma_i(x_{t_{det},i})$  is the positive score of one TP detection. Between  $\sigma_i(x_{t_{FA,start},i}) = \xi$  and  $\sigma_i(x_{t_{FA,end},i}) = 0$  the score  $\sigma_i$  follows a linear declining function, where  $\xi$  is the maximum positive score of one TP detection. For each missed FA event a negative score of  $\eta$  is considered according to

$$\zeta_{FN} = -\eta \cdot FN_1. \quad (31)$$

The scoring function  $\zeta_{FP}$  is represented by a moved negative exponential function given as

$$\zeta_{FP} = -\gamma \cdot \exp\left(\frac{-FP_1}{v}\right) - v, \quad (32)$$

where  $\gamma$  is the maximum negative score of a FP detection. As mentioned previously  $\gamma \ll \xi$ . The parameters  $\nu$  and  $\nu$  allow for additional adjustments of the score to the dataset. The negative exponential decline considers that the first FP detections will have a stronger negative impact on the performance, while for subsequent FPs the additional negative impact is small. The final  $FAD$  score is normalized with  $FAD_{\text{norm}} \in [0; 1]$  according to

$$FAD_{\text{norm}} = \frac{FAD - FAD_{\text{null}}}{FAD_{\text{opt}} - FAD_{\text{null}}}, \quad (33)$$

where  $FAD_{\text{null}}$  is the  $FAD$  score without any detection and  $FAD_{\text{opt}}$  the  $FAD$  score under optimal detection. In this work, the parameters are selected to  $\xi = 1$ ,  $\eta = 1$ ,  $\gamma = 0.05$ ,  $\nu = 10000$  and  $\nu = 0$ .

#### 4.2.2. OS event classification metrics

The performance evaluation of the OS classification of FA events is based on the  $F_1$  score according to (25). However, for the OS problem the number of classes should only be determined by the known classes. Considering all of the unknown classes as a single additional class in the test dataset would result in a biased performance result: If the problem is treated in the same way as a CS scenario, rejected samples of unknown classes would be considered as TPs - although no training samples of the unknown classes existed. Instead, the calculation of precision and recall is given by

$$Pr = \frac{\sum_{l=1}^K TP_l}{\sum_{l=1}^K (TP_l + FP_l)}, \text{ and } Re = \frac{\sum_{l=1}^K TP_l}{\sum_{l=1}^K (TP_l + FN_l)}, \quad (34)$$

where  $K$  is the number of known classes from the training dataset. In Subsection 5.2 the influence of the number of unknown event classes on the classification performance will be evaluated, which requires the definition of the *openness* of a test dataset. In [25] the authors introduce a formal definition of the openness  $O$  of a dataset according to

$$O = 1 - \sqrt{\frac{2 \times |\text{training classes}|}{|\text{testing classes}| + |\text{target classes}|}}, \quad (35)$$

with  $O \in [0; 1]$ . Large values for  $O$  correspond to a higher number of unknown classes in the dataset, while for the CS problem  $O = 0$ .

## 5. Results and discussion

In this section the performance evaluation of the proposed models for unsupervised detection and OS classification of FA events is presented. In Subsection 5.1 the proposed Persistence detector is compared to various other models, introduced in Subsection 3.1. Subsection 5.2 investigates the OS classification of FA events based on the introduced EVM model (Subsection 3.2.2). The classification performance is compared to a CS classifier benchmark. The performance evaluation is conducted based on the dataset and performance metrics from Section 4.

### 5.1. Unsupervised FA event detection

In Fig. 5 the maximum  $F_1$  score  $F_{1,\text{max}}$  and  $FAD$  score  $FAD_{\text{max}}$  at the optimal threshold  $\tau_{\text{opt},F_1}$  and  $\tau_{\text{opt},FAD}$ , respectively, are depicted together with the  $AUCPR$  for Persistence, HTM, ARIMA, SR and CNN detector. From the comparison of  $F_{1,\text{max}}$  and  $AUCPR$  it can be derived that Persistence, ARIMA, SR and CNN detector lie in the same performance range. However, the HTM detector shows a significantly poorer performance. While according to the  $F_1$  score the Persistence, ARIMA and CNN detector achieve the best detection results, with  $F_{1,\text{max}} = 0.71$ , in accordance with the  $AUCPR$  the SR detector outperforms all other detectors with  $AUCPR = 0.69$ . Interestingly, with a difference of 4 percentage points the  $F_1$  score shows a significant poorer detection performance for the SR detector. Although both the  $F_1$  score and  $AUCPR$  are performance metrics specifically tailored to scenarios with highly imbalanced classes and higher emphasis on the positive class, they suggest different results. This again motivates the need for a scenario-specific performance metric. Based on the comparison of the maximum  $FAD$  score  $FAD_{\text{max}}$  in Fig. 5 it can be concluded that both the ARIMA and CNN detector achieve the best result for the problem of real-time detection of FA events in aggregated load data with  $FAD_{\text{max}} = 0.7$ . On the contrary, with  $FAD_{\text{max}} = 0.6$  the SR detector shows a significant poorer performance in the given case of FA event detection. However, according to  $F_{1,\text{max}}$  and  $AUCPR$  the SR detector can potentially keep up with or even outperform other detection methods in scenarios with other requirements. With  $FAD_{\text{max}} = 0.69$  the performance of the Persistence detector is only slightly below the best  $FAD$  scores achieved by the ARIMA and CNN detector. As can be seen in Fig. 4 FA events in the given dataset are fast-ramped events that are characterized by a steep slope at the beginning and end of an event, resulting in a large deviation between  $x_t$  and  $x_{t-1}$ . In case of the Persistence detector this large deviation directly translates to a large anomaly score according to (1). Given that the Persistence detector can keep up with the more complex detectors regardless of the considered performance metrics, it can be concluded that the Persistence detector constitutes a trivial but effective method for detection of fast-ramped FA events.

In Fig. 6 the average detection delay  $\bar{\delta}_{\text{det}}$  is shown as a function of the threshold  $\tau$  for all detectors. As for  $\tau = 0$  all data points are declared an event, the average detection delay is  $\bar{\delta}_{\text{det}} = 0$  for all detectors. It can be seen that the HTM detector has the lowest detection delay for thresholds  $\tau > 0.1$ . The comparatively high early detection capability also explains the reduced performance discrepancy between the HTM and the other detectors for  $FAD_{\text{max}}$  compared to  $F_{1,\text{max}}$  and  $AUCPR$  (Fig. 5). While for the  $FAD$  score the contribution of TPs is weighted based on the detection delay,  $F_{1,\text{max}}$  and  $AUCPR$  do not take early detection capability into account.

The Persistence, ARIMA, SR and CNN detector show a similar  $\bar{\delta}_{\text{det}}$  for  $\tau < 0.4$ . For thresholds  $\tau > 0.4$  the SR detector shows a significantly higher detection delay, while



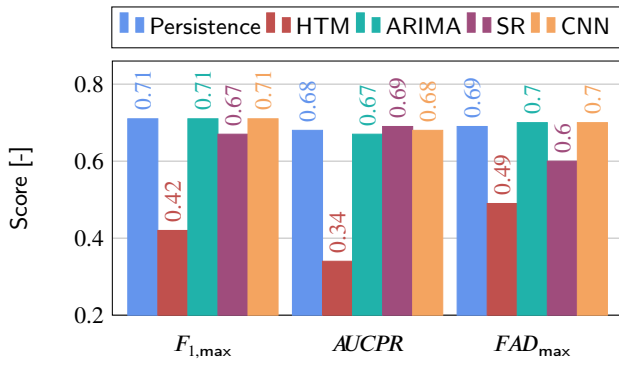


**Figure 5:** Maximum  $F_1$  score ( $F_{1,max}$ ),  $AUCPR$  and maximum  $FAD$  score ( $FAD_{max}$ ) for Persistence, HTM, ARIMA, SR and CNN detector.

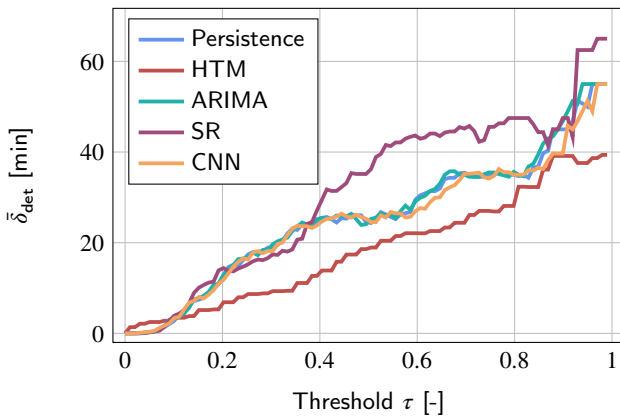


**Figure 6:** Average detection delay  $\bar{\delta}_{det}$  for Persistence, HTM, ARIMA, SR and CNN detector.

Persistence, ARIMA and CNN detector continuously show a similar detection delay.

Fig. 7 compares the average detection delay  $\bar{\delta}_{det}$  of all detectors at the optimal threshold  $\tau_{opt,FAD}$  corresponding to  $FAD_{max}$ . Although the HTM detector has the lowest average detection delay over the largest range of  $\tau$  (Fig. 6), at an operating point relevant for the considered scenario (i.e. at  $FAD_{max}$ ), it has a significantly higher detection delay compared to other detectors. The HTM detector requires a higher threshold compared to the other detectors (see Fig. 8 (c)), due to the particularly strong vulnerability to high FP numbers for low thresholds. The higher threshold in turn explains the higher average detection delay of the HTM detector. The SR detector with  $\bar{\delta}_{det} = 11.42$  min has by far the highest detection delay. Persistence, ARIMA and CNN detector show similar delays. In fact, the proposed Persistence detector shows the lowest detection delay with  $\bar{\delta}_{det} = 7.41$  min. However, it has to be considered, that the calculation of the average detection delay is only based on detected events according to (28). Thus, detecting additional events close to the end of an event (as done by ARIMA and CNN detector) results in an improved  $FAD$  score, as negative FN

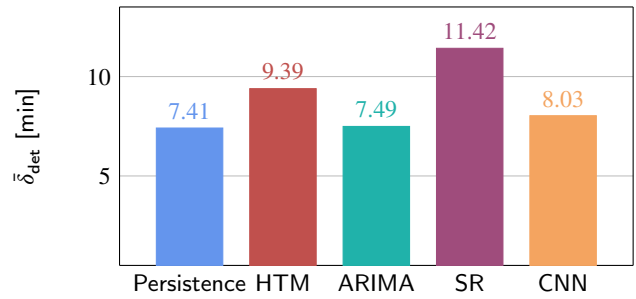


**Figure 7:** Average detection delay  $\bar{\delta}_{det}$  at  $FAD_{max}$  for Persistence, HTM, ARIMA, SR and CNN detector.

scores are avoided, even though the average detection delay increases.

Fig. 8 (a) and (b) show the  $F_1$  score over the threshold  $\tau$  and the precision-recall curve for the different detectors, respectively. Both on the  $F_1$  score and precision-recall curve a strong similarity of the Persistence, ARIMA and CNN detector can be noticed. This can be explained by the signal-to-noise ratio of the dataset. Although aggregated, the load data under investigation show a comparatively low signal-to-noise ratio due to fluctuations, introduced by unforeseeable customer behavior, and the high resolution of the data. Because of the low signal-to-noise ratio it is difficult for more complex methods, such as the applied ARIMA and CNN model, to extract additional information from the dataset compared to the trivial persistence forecast. Thus, the explainability of the dataset can be exploited by the persistence forecast to a large extent, explaining the similarity of the Persistence, ARIMA and CNN detector. However, the SR detector clearly shows a different behavior. This is due to the different mathematical approach of transforming the dataset from time into the frequency domain.

Fig. 8 (b) shows that, compared to all other detectors, the SR detector is able to keep the precision on a higher level for an increasing recall. While a high precision is not seen as an important requirement for the considered scenario, the SR detector may have advantages over the other detectors in scenarios with different requirements. Interestingly, the HTM detector clearly shows a different behavior compared to the Persistence, ARIMA and CNN detectors, even though it is also based on a time series forecast. This can partly be explained by the internal calculation of the anomaly score, which differs from the external calculation used for Persistence, ARIMA and CNN detector (see Subsection 3.1.2). However, the comparatively poor detection performance also indicates a poor underlying forecast that is even outperformed by a trivial persistence forecast. A potential reason could be insufficient adaption of the various model parameters to the dataset and scenario. Although the authors of HTM claim the provided set of parameters to be the best for anomaly detection, it may not be sufficiently appropriate for the given scenario. However, as explained before, due to the low signal-to-noise ratio, it can be expected that even extensive parameter tuning will not result in a significantly

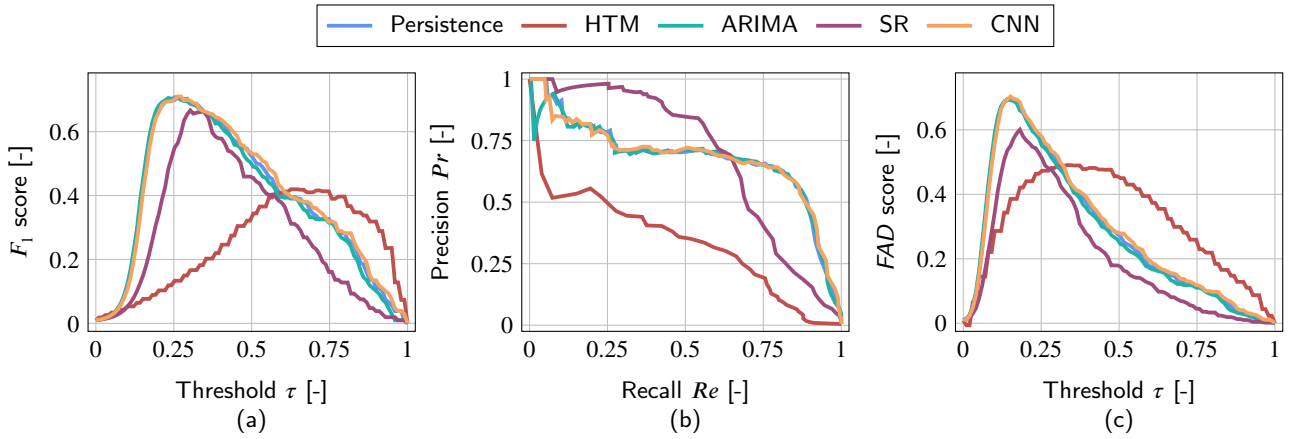


**Figure 8:** (a):  $F_1$  score, (b): Precision-recall curve, (c):  $FAD$  score for Persistence, HTM, ARIMA, SR and CNN detector.

better forecast compared to the persistence forecast.

Fig. 8 (c) shows the  $FAD$  score for all detectors over the threshold  $\tau$ . By comparing the  $F_1$  score with the  $FAD$  score, a shift between the optimal threshold  $\tau_{\text{opt},F_1}$  and  $\tau_{\text{opt},FAD}$  towards smaller values can be noticed. A smaller threshold increases the number of TPs and results in earlier detection of an event. At the same time, the number of FPs increases as well. However, as described in Subsection 4.2.1 the  $FAD$  score emphasises early event detection and weights FPs low compared to FNs, explaining the decrease of the optimal threshold. Based on the  $FAD$  score an optimal threshold for the proposed Persistence detector of  $\tau_{\text{opt},FAD} = 0.16$  is determined. At  $\tau_{\text{opt},FAD}$  191 of 205 FA events (93%) are detected by the Persistence detector, while 498 data points of all 39827 data points outside the event and rebound windows (1.25%) are falsely declared as event.

As previously described, for the dataset and scenario under investigation, more sophisticated models such as ARIMA and CNN only achieve minor improvements of the forecast compared to the persistence forecast. This also translates to a similar characteristic of the  $FAD$  score curve over the threshold  $\tau$ . It can be inferred, that for the detection of fast-ramped FA events an upper performance limit should exist at an  $FAD$  score of roughly  $FAD \approx 0.7$ . This performance limit can approximately be reached with the proposed Persistence detector ( $FAD_{\text{max}} = 0.69$ ). More advanced detection methods, such as the ARIMA and CNN detectors, only slightly improve the detection performance, but require a significantly higher maintenance and computational effort. The Persistence detector is therefore proposed to avoid frequent time and computation intensive model re-training. As described in Section 2 this is considered a great advantage in a scenario of edge computing-based distributed event detection with time and resource constraints.

## 5.2. OS classification of FA events

In Fig. 9 the confusion matrix for the EVM model applied on the OS test dataset is depicted. Besides the two known event classes FA and NO, three unknown event classes are included in the test dataset, namely MP, FV and DU,

which are summarized as "unknown". The test dataset in total contains 63 observations with  $N_{FA} = 21$ ,  $N_{NO} = 21$ ,  $N_{MP} = 7$ ,  $N_{FV} = 7$ ,  $N_{DU} = 7$ . The test dataset has an openness of  $O = 24.7\%$ . From Fig. 9 it can be derived that the EVM is able to correctly classify 90% of the FA events and 76% of the NO events. Moreover, the EVM successfully rejects 71% of all observations of the unknown classes. It can be concluded, that the EVM in principle is able to differentiate between FA and NO observations also in an OS scenario with an acceptable performance. However, the EVM also wrongly classifies 29% of the observations from the unknown classes as FA event, which reduces the precision for FA events. The precision for NO events is not affected by the unknown event classes. Also the recall of the FA and NO event classes are negatively influenced, since 10% of the FA events and 19% of the NO events, respectively, are rejected. In general, Fig. 9 demonstrates that the influence of the unknown classes on precision and recall of a class is higher compared to the influence of the other known class.

|                  |         |                       |           |           |
|------------------|---------|-----------------------|-----------|-----------|
| True event class | FA      | 19<br>90%             | 0<br>0%   | 2<br>10%  |
|                  | NO      | 1<br>5%               | 16<br>76% | 4<br>19%  |
|                  | unknown | 6<br>29%              | 0<br>0%   | 15<br>71% |
|                  |         | FA                    | NO        | unknown   |
|                  |         | Predicted event class |           |           |

**Figure 9:** Confusion matrix of the EVM model on the OS classification test dataset with an openness  $O = 24.7\%$ .

In order to investigate the benefit of applying an OS clas-

sifier in the more realistic scenario with presence of unknown classes, the performance is compared to a CS classifier. For this purpose, the EVM model is applied on the test dataset as both an OS and CS classifier. In the CS setting the rejection of observations with  $\hat{P}(C_i|v') < 0.9$  is deactivated and observations are classified according to  $\hat{P}(C_i|v')$ . Moreover, in order to investigate the influence of the number of unknown classes, the comparison are conducted on a test dataset with increasing fractions of unknown classes. In Fig. 10 the comparison of the OS and CS EVM for a varying openness  $O$  of the test dataset is depicted. The performance is evaluated

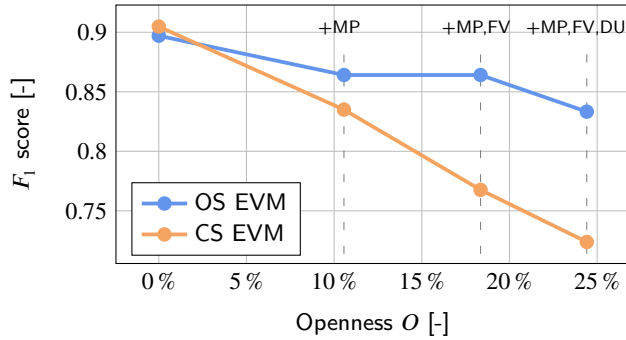


**Figure 10:** Comparison of the  $F_1$  score between OS and CS EVM model on the OS classification problem with a varying openness  $O$ .

based on the  $F_1$  score. For the CS problem ( $O = 0$ ) the performance of the CS classifier is slightly better compared to the OS classifier, since the OS classifier wrongly rejects some of the observations of the known classes. By adding MP events as unknown class to the test dataset the openness of the test dataset increases to  $O = 10.56\%$ . In this scenario the OS classifier outperforms the CS classifier. While the OS classifier is capable of rejecting observations from unknown classes the CS classifier assigns all observations of unknown classes to one of the known classes, resulting in a decreased precision. However, the performance of the OS EVM decreases as well. This is due to two reasons: First, not all observations from the unknown classes are successfully rejected. Second, being capable of rejecting observations can also lead to falsely rejected observations of known classes. Nevertheless, for the investigated scenario of FA event classification the rejection capability improves the performance compared to the CS classifier already for the existence of only one unknown class. Extending the test dataset with the unknown FV event class ( $O = 18.35\%$ ) has no influence on the performance of the OS EVM. This can be explained by the specific characteristic of FV events. The number of zeros  $n_0$  constitutes a strong differentiator for observations of the FV event class, making it comparatively easy for the OS EVM to differentiate between FV and the known FA and NO events. Nevertheless, the  $F_1$  score of the CS classifier further decreases from  $F_1 = 0.835$  to  $F_1 = 0.768$  since all observations of the FV event class are assigned to either the FA or NO event class. In the final scenario ( $O = 24.7\%$ )

all unknown event classes are added to the test dataset, corresponding to the scenario described by Fig. 9. Adding the unknown DU event class further decreases the performance for both the OS and CS classifier. However, while for the CS EVM the  $F_1$  score decreases by 4.38 percent, the OS classifier only shows a decrease of 3.08 percent. In summary, the performance of the OS EVM decreased from  $F_1 = 0.897$  ( $O = 0\%$ ) to  $F_1 = 0.833$  ( $O = 24.7\%$ ), while the CS classifier performance decreased from  $F_1 = 0.905$  ( $O = 0\%$ ) to  $F_1 = 0.724$  ( $O = 24.7\%$ ). This demonstrates that the rejection capability of the OS classifier allows maintaining the classification performance on a higher level, for increasing fractions of unknown classes. Nevertheless, also for the OS classifier the performance deteriorates with additional unknown classes.

To summarize, FA events can be classified also in the more realistic OS scenario and applying OS classifiers can significantly improve the performance under these conditions. However, the classification performance of the EVM is expandable, due to the very limited training data. The size of the dataset constitutes a limitation of the presented study, since the small number of observations and classes prevent more comprehensive investigations. Nevertheless, this study proves the fundamental feasibility of OS classification of FA events on real data.

## 6. Conclusion and future work

This work demonstrates the fundamental feasibility of unsupervised detection and OS classification of FA events. A data processing pipeline for FA event identification is proposed. The method combines unsupervised event detection and OS classification. A simple Persistence detector is proposed and implemented as unsupervised event detector. The comparison to more complex and computational expensive detection models demonstrates a comparable performance and the existence of an upper performance limit. As OS classifier the EVM is used. It is shown that the use of an OS classifier significantly improves the classification performance in the more realistic OS scenario compared to a traditional CS classifier. Both the Persistence detector and EVM classifier are selected with a view to an application in a distributed event detection architecture with time and resource constraints due to edge computing. This work demonstrates that the main building blocks of the proposed pipeline can be realised with comparatively simple methods that fulfill important requirements for an application in a distributed event detection architecture.

Given the fundamental proof of the main building blocks, a logical next step is the investigation of the coupling of the Persistence detector and EVM classifier in the proposed EIP for FA events. Moreover, for both the detection as well as classification step, several possible improvements could be investigated. One direction could be the integration of additional regressors for unsupervised event detection such as temperature and solar radiation. For the OS classification problem principle component analysis or other methods for dimensionality reduction could be applied to reduce the fea-

---

**Algorithm 1** General procedure of the EIP for FA events.

---

```
1: for new incoming data point  $x_{\Delta,t}$  do:
2:   PERSISTENCE_FORECAST( $x_{\Delta,t}$ ) ▷ Start of unsupervised event detection
3:   return  $\hat{x}_{\Delta,t}$ 
4:   if  $|\hat{x}_{\Delta,t} - x_{\Delta,t}| < \tau$  then:
5:     Declare  $x_{\Delta,t}$  normal behavior
6:   else:
7:     Declare  $x_{\Delta,t}$  an event
8:     BACKWARD_SAMPLING( $x_{\Delta,t}$ ) ▷ Start of event sampling
9:     return  $\mathbf{x}_{\Delta,bw} = \{x_{\Delta,t-w_x}, \dots, x_{\Delta,t+e}\}$ 
10:    FORWARD_SAMPLING( $x_{\Delta,t}$ )
11:    if another event at  $x_{\Delta,t+a} \in \{x_{\Delta,t+1}, \dots, x_{\Delta,t+w_x}\}$  then:
12:      return  $\mathbf{x}_{\Delta,fw} = \{x_{\Delta,t-e}, \dots, x_{\Delta,t+a+e}\}$ 
13:    else:
14:      return  $\mathbf{x}_{\Delta,fw} = \{x_{\Delta,t-e}, \dots, x_{\Delta,t+w_x}\}$ 
15:    for  $\mathbf{x}$  in  $[\mathbf{x}_{\Delta,bw}, \mathbf{x}_{\Delta,fw}]$  do:
16:      Calculate feature vector  $v = [\mu_x, \sigma_x, x_{\min}, x_{\max}, n_0, n_{\minmax}]$ 
17:      EXTREME_VALUE_MACHINE( $v$ ) ▷ Start of OS classification
18:      return  $P(C_{flexibility}|v), P(C_{normal\_behavior}|v)$ 
19:      if  $P(C_{flexibility}|v) \geq P(C_{normal\_behavior}|v)$  and  $\geq \rho$  then:
20:        Declare sample  $\mathbf{x}$  as flexibility activation event
21:      else if  $P(C_{flexibility}|v) \leq P(C_{normal\_behavior}|v)$  and  $\geq \rho$  then:
22:        Declare sample  $\mathbf{x}$  as normal behavior
23:      else:
24:        Declare sample  $\mathbf{x}$  as unknown event
```

---

ture space dimension while retaining majority of the information. Finally, the proposed pipeline could be extended from FA event identification to identification of multiple relevant events in active DGs.

## Acknowledgement

The authors would like to acknowledge the financial support of RegSys18 91363 HONOR.

## Appendix

### References

- [1] European Commission. Impact assessment on stepping up europe's 2030 climate ambition. investing in a climate-neutral future for the benefit of our people. 2020.
- [2] Chun-Hao Lo and Nirwan Ansari. Decentralized controls and communications for autonomous distribution networks in smart grid. *IEEE Transactions on Smart Grid*, 4(1):66–77, 2013. doi: 10.1109/TSG.2012.2228282.
- [3] Junhui Zhao, Caisheng Wang, Bo Zhao, Feng Lin, Quan Zhou, and Yang Wang. A review of active management for distribution networks: current status and future development trends. *Electric Power Components and Systems*, 42(3-4):280–293, 2014.
- [4] Konstantinos Spiliotis, Ariana Isabel Ramos Gutierrez, and Ronnie Belmans. Demand flexibility versus physical network expansions in distribution grids. *Applied Energy*, 182:613–624, 2016.
- [5] Peter Richardson, Damian Flynn, and Andrew Keane. Impact assessment of varying penetrations of electric vehicles on low voltage distribution systems. In *IEEE PES General Meeting*, pages 1–6, 2010. doi: 10.1109/PES.2010.5589940.
- [6] Hang Zhang, Bo Liu, and Hongyu Wu. Smart grid cyber-physical attack and defense: A review. *IEEE Access*, 9:29641–29659, 2021. doi: 10.1109/ACCESS.2021.3058628.
- [7] Angel Esteban Labrador Rivas and Taufik Abrão. Faults in smart grid systems: Monitoring, detection and classification. *Electric Power Systems Research*, 189:106602, 2020. doi: <https://doi.org/10.1016/j.epsr.2020.106602>.
- [8] Mohammed Kemal, Ruben Sanchez, Rasmus Olsen, Florin Iov, and Hans-Peter Schwefel. On the trade-off between timeliness and accuracy for low voltage distribution system grid monitoring utilizing smart meter data. *International Journal of Electrical Power & Energy Systems*, 121:106090, 2020.
- [9] Dhirender Singh, R. K. Banyal, and Arvind Kumar Sharma. Cloud computing research issues, challenges, and future directions. In Vijay Singh Rathore, Marcel Worring, Durgesh Kumar Mishra, Amit Joshi, and Shikha Maheshwari, editors, *Emerging Trends in Expert Applications and Security*, pages 617–623, Singapore, 2019. Springer Singapore. ISBN 978-981-13-2285-3.
- [10] Ashkan Yousefpour, Caleb Fung, Tam Nguyen, Krishna Kadiyala, Fatemeh Jalali, Amirreza Niakanlahiji, Jian Kong, and Jason P. Jue. All one needs to know about fog computing and related edge computing paradigms: A complete survey. *Journal of Systems Architecture*, 98:289–330, 2019. doi: <https://doi.org/10.1016/j.sysarc.2019.02.009>.
- [11] Joao Pereira and Margarida Silveira. Unsupervised anomaly detection in energy time series data using variational recurrent autoencoders with attention. In *2018 17th IEEE International Conference on Machine Learning and Applications (ICMLA)*, pages 1275–1282. IEEE, 2018.
- [12] Anomadarshi Barua, Deepan Muthirayan, Pramod P Khargonekar, and Mohammad Abdullah Al Faruque. Hierarchical temporal memory based one-pass learning for real-time anomaly detection and simultaneous data prediction in smart grids. *IEEE Transactions on Dependable and Secure Computing*, 2020.
- [13] Keith Hollingsworth, Kathryn Rouse, Jin Cho, Austin Harris, Mina Sartipi, Sevin Sozer, and Bryce Enevoldson. Energy anomaly detection with forecasting and deep learning. In *2018 IEEE International Conference on Big Data (Big Data)*, pages 4921–4925. IEEE, 2018.
- [14] Bijay Neupane, Torben Bach Pedersen, and Bo Thiesson. Towards flexibility detection in device-level energy consumption. In *Internation*



- tional Workshop on Data Analytics for Renewable Energy Integration*, pages 1–16. Springer, 2014.
- [15] Elena Mocanu, Phuong H Nguyen, and Madeleine Gibescu. Energy disaggregation for real-time building flexibility detection. In *2016 IEEE Power and Energy Society General Meeting (PESGM)*, pages 1–5. IEEE, 2016.
  - [16] Yikui Liu, Lei Wu, and Jie Li. D-pmu based applications for emerging active distribution systems: A review. *Electric Power Systems Research*, 179:106063, 2020. doi: 10.1016/j.epsr.2019.106063.
  - [17] Imene Mitiche, Alan Nesbitt, Stephen Conner, Philip Boreham, and Gordon Morison. 1d-cnn based real-time fault detection system for power asset diagnostics. *IET Generation, Transmission & Distribution*, 14(24):5766–5773, 2020.
  - [18] I. Niazazari and H. Livani. Disruptive event classification using pmu data in distribution networks. In *IEEE Power & Energy Society, editor, 2017 IEEE Power & Energy Society General Meeting*, pages 1–5, New York, 2018. IEEE. ISBN 978-1-5386-2212-4. doi: 10.1109/PESGM.2017.8274154.
  - [19] Desiree Phillips and Thomas Overbye. Distribution system event detection and classification using local voltage measurements. In *PECI 2014*, pages 1–4, [Piscataway, N.J.], 2014. IEEE. ISBN 978-1-4799-4881-9. doi: 10.1109/PECI.2014.6804576.
  - [20] Subutai Ahmad, Alexander Lavin, Scott Purdy, and Zuha Agha. Unsupervised real-time anomaly detection for streaming data. *Neurocomputing*, 262:134–147, 2017. doi: 10.1016/j.neucom.2017.04.070.
  - [21] Asrul H Yaacob, Ian KT Tan, Su Fong Chien, and Hon Khi Tan. Arima based network anomaly detection. In *2010 Second International Conference on Communication Software and Networks*, pages 205–209. IEEE, 2010.
  - [22] Tolga Ergen and Suleyman Serdar Kozat. Unsupervised anomaly detection with lstm neural networks. *IEEE transactions on neural networks and learning systems*, 31(8):3127–3141, 2019.
  - [23] Mohsin Munir, Shoaib Ahmed Siddiqui, Andreas Dengel, and Sheraz Ahmed. Deepant: A deep learning approach for unsupervised anomaly detection in time series. *IEEE Access*, 7:1991–2005, 2019. doi: 10.1109/ACCESS.2018.2886457.
  - [24] Hansheng Ren, Bixiong Xu, Yujing Wang, Chao Yi, Congrui Huang, Xiaoyu Kou, Tony Xing, Mao Yang, Jie Tong, and Qi Zhang. Time-series anomaly detection service at microsoft. In Ankur Teredesai, editor, *Proceedings of the 25th ACM SIGKDD International Conference on Knowledge Discovery & Data Mining*, ACM Digital Library, pages 3009–3017, New York, NY, United States, 2019. Association for Computing Machinery. ISBN 9781450362016. doi: 10.1145/3292500.3330680.
  - [25] Walter J. Scheirer, Anderson de Rezende Rocha, Archana Sapkota, and Terrance E. Boulton. Toward open set recognition. *IEEE transactions on pattern analysis and machine intelligence*, 35(7):1757–1772, 2013. doi: 10.1109/TPAMI.2012.256.
  - [26] Abhijit Bendale and Terrance Boulton. Towards open world recognition. In *Proceedings of the IEEE conference on computer vision and pattern recognition*, pages 1893–1902, 2015.
  - [27] Ethan M. Rudd, Lalit P. Jain, Walter J. Scheirer, and Terrance E. Boulton. The extreme value machine. *IEEE transactions on pattern analysis and machine intelligence*, 40(3):762–768, 2018. doi: 10.1109/TPAMI.2017.2707495.
  - [28] Chuanxing Geng and Songcan Chen. Collective decision for open set recognition. *IEEE Transactions on Knowledge and Data Engineering*, page 1, 2020. doi: 10.1109/TKDE.2020.2978199.
  - [29] Chuanxing Geng, Sheng-jun Huang, and Songcan Chen. Recent advances in open set recognition: A survey. *IEEE Transactions on Pattern Analysis and Machine Intelligence*, PP:1, 2020. doi: 10.1109/TPAMI.2020.2981604.
  - [30] Ashish Gupta, Hari Prabhat Gupta, Bhaskar Biswas, and Tanima Dutta. Approaches and applications of early classification of time series: A review. 2020. doi: 10.1109/TAI.2020.3027279.
  - [31] Charalampos Ziras, Carsten Heinrich, and Henrik W. Bindner. Why baselines are not suited for local flexibility markets. *Renewable and Sustainable Energy Reviews*, 135:110357, 2021. doi: 10.1016/j.rser.2020.110357.
  - [32] Torsten Suel. Delta compression techniques. *Encyclopedia of Big Data Technologies*, 63, 2019.
  - [33] Jeff Hawkins and Sandra Blakeslee. *On intelligence*. Macmillan, 2004.
  - [34] Chirag Deb, Fan Zhang, Junjing Yang, Siew Eang Lee, and Kwok Wei Shah. A review on time series forecasting techniques for building energy consumption. *Renewable and Sustainable Energy Reviews*, 74:902–924, 2017. doi: https://doi.org/10.1016/j.rser.2017.02.085.
  - [35] Hyndman, R. J. Forecasting with long seasonal periods. <https://robjhyndman.com/hyndsight/longseasonality/>, 2010. [Online; accessed: 23/07/2021].
  - [36] Taylor G. Smith et al. pmdarima: Arima estimators for Python, 2017–. URL [https://alkaline-ml.com/pmdarima/modules/generated/pmdarima.arima.auto\\_arima.html](https://alkaline-ml.com/pmdarima/modules/generated/pmdarima.arima.auto_arima.html). [Online; accessed 23/07/2021].
  - [37] Keiron O’Shea and Ryan Nash. An introduction to convolutional neural networks. *arXiv preprint arXiv:1511.08458*, 2015.
  - [38] Quoc V Le et al. A tutorial on deep learning part 2: Autoencoders, convolutional neural networks and recurrent neural networks. *Google Brain*, 20:1–20, 2015.
  - [39] Geoffrey E Hinton, Nitish Srivastava, Alex Krizhevsky, Ilya Sutskever, and Ruslan R Salakhutdinov. Improving neural networks by preventing co-adaptation of feature detectors. *arXiv preprint arXiv:1207.0580*, 2012.
  - [40] Xiaodi Hou and Liqing Zhang. Saliency detection: A spectral residual approach. In *2007 IEEE Conference on computer vision and pattern recognition*, pages 1–8. Ieee, 2007.
  - [41] Yu-Fei Ma and Hong-Jiang Zhang. Contrast-based image attention analysis by using fuzzy growing. In *Proceedings of the eleventh ACM international conference on Multimedia*, pages 374–381, 2003.
  - [42] Yun Zhai and Mubarak Shah. Visual attention detection in video sequences using spatiotemporal cues. In *Proceedings of the 14th ACM international conference on Multimedia*, pages 815–824, 2006.
  - [43] Yang Yu, Wei-Yang Qu, Nan Li, and Zimin Guo. Open-category classification by adversarial sample generation.
  - [44] Steven W Smith et al. *The scientist and engineer’s guide to digital signal processing*, volume 14. California Technical Pub. San Diego, 1997.
  - [45] Carsten Heinrich, Charalampos Ziras, Angeliki L.A. Syri, and Henrik W. Bindner. Ecogrid 2.0: A large-scale field trial of a local flexibility market. *Applied Energy*, 261:114399, 2020. doi: <https://doi.org/10.1016/j.apenergy.2019.114399>.